

A QUANTUM REPEATER BASED ON DECOHERENCE FREE SUBSPACES

UWE DORNER

*Clarendon Laboratory, University of Oxford, Parks Road
Oxford OX1 3PU, United Kingdom*

ALEXANDER KLEIN

*Clarendon Laboratory, University of Oxford, Parks Road
Oxford OX1 3PU, United Kingdom*

DIETER JAKSCH

*Clarendon Laboratory, University of Oxford, Parks Road
Oxford OX1 3PU, United Kingdom*

We study a quantum repeater which is based on decoherence free quantum gates recently proposed by Klein *et al.* [Phys. Rev. A, **73**, 012332 (2006)]. A number of operations on the decoherence free subspace in this scheme makes use of an ancilla qubit, which undergoes dephasing and thus introduces decoherence to the system. We examine how this decoherence affects entanglement swapping and purification as well as the performance of a quantum repeater. We compare the decoherence free quantum repeater with a quantum repeater based on qubits that are subject to decoherence and show that it outperforms the latter when decoherence due to long waiting times of conventional qubits becomes significant. Thus, a quantum repeater based on decoherence free subspaces is a possibility to greatly improve quantum communication over long or even intercontinental distances.

Keywords: Quantum communication, Quantum repeater, Quantum networks, Decoherence free subspace, Noise in quantum systems

1 Introduction

Quantum communication is one of the experimentally most advanced areas of quantum information processing and promises to yield commercial applications in the near future [1]. In addition to free space quantum communication, current setups mainly use photon transmission in optical fibers and the distances over which quantum cryptography is possible so far are in the range of up to about 100km [2]. However, quantum communication over longer distances is primarily limited by photon loss, which grows exponentially with the length of the fibre. A possible solution of this problem is the use of quantum repeaters [3, 4] to distribute maximally entangled pairs of qubits over long distances. These pairs can then be used for entanglement based quantum communication by teleporting [5] quantum information from

one party to the other. The basic idea of a quantum repeater is to divide the transmission line into shorter segments with a length of the order of the attenuation length of the fibre. On each segment entangled particle pairs are created and by applying entanglement swapping [6] and purification protocols [7, 8, 3] entangled pairs of larger distances are produced. Successive application of these steps according to a nested repeater protocol [3] creates a distant qubit pair with high entanglement fidelity.

During the purification process the entanglement fidelity of a pair of qubits is successively increased by sacrificing auxiliary entangled pairs. In the present paper we will use a purification protocol known as “entanglement pumping” [9]. From a practical point of view the use of entanglement pumping is favourable compared to other purification schemes [7, 8, 10] since it requires significantly fewer qubits and thus might be easier to implement. However, the decrease of physical resources comes at the cost of long operation times of the repeater during which quantum information has to be stored. These waiting times grow quickly with the distance of the two parties who desire to share an entangled state and if they are too long the stored quantum information will decohere to such a degree that the quantum repeater can not be successfully operated anymore. This problem was recently addressed by Hartmann *et al.* [11] (see also [12]), who examined the limitations of a quantum repeater (in terms of maximal distance) depending on the noise strength. A number of modifications of the repeater protocol have been proposed and it was shown that the maximal distance might be increased by an order of magnitude at the cost of a reasonable overhead of resources. Unlimited distances are only possible with the help of quantum error correction. However, this imposes very stringent error thresholds, which seem out of reach with present technology.

In this paper we pursue the different and conceptually more straightforward strategy of improving the quality of the quantum memories at the repeater nodes. We study a repeater architecture based on a scheme recently proposed by Klein *et al.* [13], which relies on the concept of decoherence free subspaces (DFSs) [14, 15, 16, 17]. DFSs are a method of passive error correction or error prevention and can significantly increase the lifetime of quantum information and reliability of quantum computing as already demonstrated in a number of experiments [18, 19, 20, 21, 22, 23, 24, 25, 26, 27]. In Ref. [13] a logical qubit at a repeater node is represented by two states of a decoherence free subspace of a Hilbert space consisting of four atomic qubits. The logical qubits are immune to collective noise thus greatly improving the lifetime of stored quantum information. However, gate operations become more complicated and slower than operations on “bare”, unprotected atomic qubits. In fact the two qubit operation proposed in [13] is not decoherence free since an unprotected auxiliary qubit is used to mediate between two logical DFS qubits. In the present work we examine how this noise affects the performance of the quantum repeater network and show that it is possible to create entangled pairs of high fidelity over intercontinental distances. We compare the results to a repeater based on unprotected qubits, i.e., qubits that are subject to decoherence, and show that it outperforms the latter when decoherence due to long waiting times becomes significant. Although we consider only the special case of a quantum repeater, we emphasise that the methods we employ are generally applicable to arbitrary quantum networks.

This paper is organised as follows. In Sec. 2 we briefly review the quantum repeater protocol. In Sec. 3 we present the error model we use for quantum repeaters based on unprotected qubits and DFS qubits. In the same section we furthermore describe the quantum

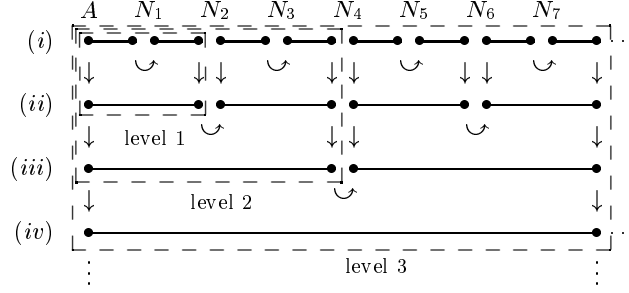


Fig. 1. Illustration of the nested repeater protocol. For explanation see text.

circuits necessary to implement the repeater. In Sec. 4 we present the results of simulations for both repeater setups. Finally we conclude in Sec. 5.

2 The quantum repeater

In this paper we use the nested repeater protocol developed in [3, 9], which consists of a combination of entanglement purification and entanglement swapping. The goal is to create a highly entangled pair between two parties, say, A and B , which might be attempted by transmitting a photon through a fibre. However, unwanted noise will decrease the entanglement fidelity of the qubit pair monotonously with the distance between A and B . The fidelity can be increased again by applying purification procedures, in which additional entangled pairs between A and B are created and sacrificed in order to distill an entangled pair with high fidelity. However, if the distance between A and B is too large, the entanglement fidelity of the pairs can drop below a minimum value f_{\min} , which is required by the purification protocol to increase the entanglement fidelity [9]. To overcome this problem, a number of intermediate nodes N_i with sufficiently small distances l_0 are introduced between A and B , and entangled qubit pairs are prepared between each of the intermediate nodes such that the entanglement fidelity of each pair is greater than f_{\min} . These pairs can be purified and connected via entanglement swapping to create an entangled pair of larger distance. For the setup used in this work we consider purification via “entanglement pumping” [9], which requires considerably less qubits than other schemes [7, 8, 10] and is thus preferable from a practical point of view.

The principle of the nested repeater protocol is illustrated by the example shown in Fig. 1: Each bullet represents a qubit and the lines between them indicate entanglement. On repeater level 1 (indicated by the dashed box on the top left) two entangled qubit pairs between nodes A and N_1 and between nodes N_1 and N_2 are created in line (i). The two qubits at node N_1 are then connected via entanglement swapping, creating an entangled pair of qubits with larger distance, indicated by the curved arrow. Within the schematic of Fig. 1 the state of this qubit pair is then transferred by a quantum operation to the qubit pair in line (ii). We then generate further entangled pairs in line (i), which are used to purify the pair in line (ii), indicated by vertical arrows. Given that l_0 is the distance between the nodes, the final pair will have a distance $2l_0$. Repeater level 2 consists of two adjacent level 1 repeaters, both of which create an entangled pair of distance $2l_0$ on line (ii). These two pairs are then connected,

the resulting pair is transferred to line (iii) and subsequently produced pairs are used to purify the pair in line (iii), which has now a distance $4l_0$. Repeater level 3 is constructed in the same way: We use two level 2 repeaters which successively generate pairs in line (iii). After connecting them the resulting pair is transferred to line (iv), and subsequently produced pairs are used to purify the pair with distance $8l_0$ in line (iv). In this example the distance between the entangled qubits is doubled with each further repeater level. In general, the number of entanglement swapping steps on each repeater level can vary from level to level and is adapted to the specific physical situation. The distance between entangled qubits on repeater level n is then given by

$$S_n \equiv l_0 \prod_{j=1}^n (L_j + 1) \quad (1)$$

for $n \geq 1$ and $S_0 = l_0$. The quantity L_j is the number of connections on level j immediately before the final qubit pair of this level is purified, i.e. in the example shown in Fig. 1 we have $L_1 = L_2 = L_3 = 1$. Thus, L_j is generally different from the total number of connections necessary to operate a level j repeater.

We note that in basically all quantum communication schemes flying qubits are represented by photons. For our setup we assume that the states of these photons are first transferred to stationary qubits (atoms) creating an entangled pair with entanglement fidelity f_0 , which might be lower than the entanglement fidelity of the photon pair. We use this fidelity f_0 as the starting fidelity in all our discussions. We also note that the state transfer described above is not necessary if we do an appropriate relabeling of the qubits. However, for reasons given in Sec. 4 we assume that this transfer is done via a quantum operation.

3 Error models

3.1 Error model for unprotected qubits

The error model we use in this paper is motivated by realisations of quantum information processing with single atoms stored in tight traps [19, 20, 13]. In this scenario, qubits can be represented by two metastable states of atoms. The lifetime of these states is typically on the order of several minutes or longer, such that their spontaneous decay can be neglected [18, 19, 20, 21, 28]. The major source of decoherence is then given by dephasing, represented by the σ_z -Pauli operator. Unitary single qubit operations necessary to manipulate the qubits can be realised by laser pulses and static magnetic or electric fields. It is thus easily possible to implement Hamiltonians which are proportional to Pauli operators such that the time evolution of the system corresponds to rotations around the x, y , and z axis of the Bloch sphere. For two qubit operations various schemes have been developed [29]. Here, we consider two qubit operations caused by an Ising interaction, which can be realised via the collisional interaction between neutral atoms stored in optical traps [30, 31].

3.1.1 Single qubit gates and measurements

We assume that the major source of noise is dephasing so that the time evolution of the system state ρ whilst applying a gate described by H_α^i on qubit i is determined by the master equation ($\hbar = 1$)

$$\dot{\rho} = -i[H_\alpha^i, \rho] + \frac{\gamma}{2}(\sigma_z^i \rho \sigma_z^i - \rho). \quad (2)$$

Here,

$$H_\alpha^i = \Omega_\alpha \sigma_\alpha^i, \quad (3)$$

where σ_α^i are the Pauli operators with $\alpha = 0, x, y, z$. In the case of $\alpha = 0$ we set $\sigma_0^i = \mathbf{1}$ so that the above master equation also describes the dephasing of a quantum channel or memory. For simplicity we furthermore assume that Ω_α is real and non-negative. For vanishing noise (i.e., $\gamma = 0$) the i th qubit undergoes a rotation around the x , y or z axis

$$\rho \rightarrow R_\alpha^i(\theta) \rho R_\alpha^i(\theta)^\dagger \quad \text{with} \quad R_\alpha^i(\theta) \equiv e^{-i\frac{\theta}{2}\sigma_\alpha^i}, \quad (4)$$

where the rotation angle is given by $\theta = 2\Omega_\alpha t$.

In the presence of dephasing (i.e., $\gamma \neq 0$) the solutions of Eq. (2) can be described by quantum operations \mathcal{E}_α^i ,

$$\rho \rightarrow \mathcal{E}_\alpha^i(\theta)[\rho] = \sum_k E_{\alpha,k}^i \rho (E_{\alpha,k}^i)^\dagger. \quad (5)$$

For $\alpha = 0$, i.e., if the commutator in Eq. (2) vanishes, the evolution of the density operator is given by

$$\rho \rightarrow \mathcal{E}_0^i(\gamma t)[\rho] = p_1(\gamma t)\rho + p_2(\gamma t)\sigma_z^i \rho \sigma_z^i, \quad (6)$$

where

$$p_1(\gamma t) = \frac{1}{2}(1 + e^{-\gamma t}), \quad p_2(\gamma t) = \frac{1}{2}(1 - e^{-\gamma t}). \quad (7)$$

Note that for $\alpha = z$ the noise operator σ_z^i commutes with H_z^i so that

$$\mathcal{E}_z^i(\theta)[\rho] = \mathcal{E}_0^i(\gamma t)[R_z(\theta)\rho R_z(\theta)^\dagger] = R_z(\theta)\mathcal{E}_0^i(\gamma t)[\rho]R_z(\theta)^\dagger, \quad (8)$$

i.e., the process can be replaced by a perfect rotation followed by noise in the channel, or vice versa. In the remainder of the present work we omit the superscript i whenever it is clear from the context (e.g. in quantum circuits) on which qubit the operation is acting on.

Non-ideal measurements are described in this paper by the positive operator valued measure [9]

$$P_0 = \eta|0\rangle\langle 0| + (1 - \eta)|1\rangle\langle 1| \quad (9)$$

$$P_1 = \eta|1\rangle\langle 1| + (1 - \eta)|0\rangle\langle 0| \quad (10)$$

with $0 \leq \eta \leq 1$. The parameter η is the probability to obtain the correct result if a measurement is done in the $\{|0\rangle, |1\rangle\}$ -basis.

3.1.2 Two qubit gates

We consider two qubit operations mediated by an Ising interaction. The dynamics of the system can thus be described by a master equation of the form

$$\dot{\rho} = -i[\Omega_{zz}\sigma_z^i\sigma_z^j, \rho] + \frac{\gamma}{2}(\sigma_z^i\rho\sigma_z^i - \rho) + \frac{\gamma}{2}(\sigma_z^j\rho\sigma_z^j - \rho), \quad (11)$$

where we assume that the noise on qubit i and j is uncorrelated. Since the Ising Hamiltonian commutes with the noise operators σ_z^i , the time evolution is simply given by

$$\rho \rightarrow \mathcal{E}_{zz}^{ij}(\xi)[\rho] = \mathcal{E}_0^i(\gamma t)[\mathcal{E}_0^j(\gamma t)[e^{-i\frac{\xi}{2}\sigma_z^i\sigma_z^j}\rho e^{i\frac{\xi}{2}\sigma_z^i\sigma_z^j}]], \quad (12)$$

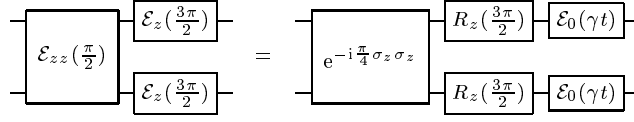


Fig. 2. Controlled-Z operation, $\mathcal{Z}_{\downarrow}^{AA}$, on two unprotected qubits. The left circuit can be replaced by an effective circuit consisting of ideal gates followed by noise in the quantum channels. The time t is given by $t = \pi/4\Omega_{zz} + 3\pi/4\Omega_z$, which is the time needed to perform the noiseless gates.

where $\xi = 2\Omega_{zz}t$. The order of the three distinct operations in the above equation is arbitrary. This means that \mathcal{E}_{zz}^{ij} can, for example, be described by a perfect operation followed by dephasing in the quantum channels. An application of this fact is illustrated in Fig. 2, which shows the realisation of a noisy controlled-Z gate on two qubits. In the following figures we denote this gate as $\mathcal{Z}_{\downarrow}^{AA}$, the superscript indicating that the gate is acting on two unprotected (atomic) qubits. The subscript defines control and target qubit, i.e., in quantum circuits the arrowhead points to the target qubit. Strictly speaking this is not necessary since this gate is symmetric under qubit exchange. However, in later sections we use a similar notation for controlled- $(-Z)$ gates which are not symmetric.

3.1.3 Building blocks of the quantum repeater using unprotected qubits

As indicated in Sec. 2, three basic modules are needed to run the quantum repeater. In particular, these are the transfer of a state from one qubit to another one, entanglement swapping, and entanglement purification. In Figs. 3-5 we show possible implementations of these three blocks according to the error models and gate operations described in Secs. 3.1.1 and 3.1.2. In our simulations qubits that are measured are immediately removed from the system by tracing them out. The removal of a qubit is indicated by a Tr -symbol in the corresponding quantum circuits unless we perform measurements that classically control further operations. Furthermore, we assume for simplicity that $\Omega \equiv \Omega_x = \Omega_y = \Omega_z$.

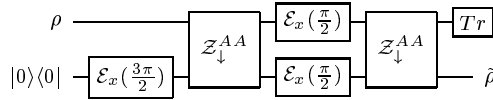


Fig. 3. State transfer between two unprotected qubits. In the noiseless case the output state $\tilde{\rho}$ would be equal to the input state ρ .

Clearly, the partitioning of the three blocks into elementary gate operations is not unique and in the presence of noise different architectures can lead to different fidelities. In our simulations we compared various possibilities, and the realisations shown in this article are the ones which led to the best results for the error models and corresponding error parameters we use, see Sec. 4. Moreover, in the case of a quantum repeater based on unprotected qubits, which is used for communication over long distances, the dominant source of noise is due to long waiting times during classical communications (see below and Ref. [11]) and the specific partitioning of the blocks becomes less important.

Apart from noise during gate operations, the quantum circuits shown in this section also include noise which is due to waiting times of qubits. Whenever it is unavoidable that a qubit

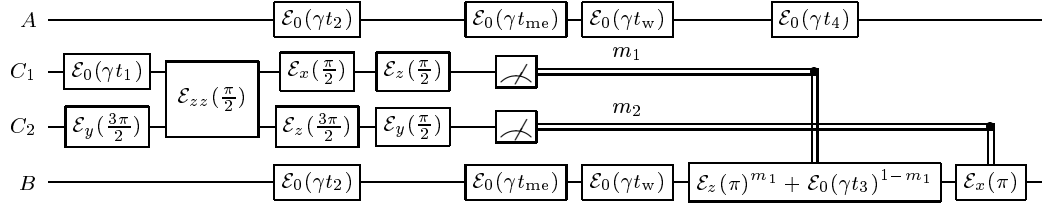


Fig. 4. Entanglement swapping of qubit pairs $A - C_1$ and $C_2 - B$. The state of qubit C_1 is teleported to qubit B by using the entanglement of qubit pair $C_2 - B$ yielding an entangled pair $A - B$. The waiting times are given by $t_1 = 3\pi/4\Omega$, $t_2 = 5\pi/4\Omega + \pi/4\Omega_{zz}$ and $t_3 = \pi/2\Omega$. The value of t_4 depends on the outcome of the measurement of qubit C_2 , given by $m_2 = 0, 1$. In particular we have $t_4 = \pi/\Omega$ if $m_2 = 1$ and $t_4 = \pi/2\Omega$ if $m_2 = 0$. The time t_{me} corresponds to the time necessary to perform a measurement and $t_w = S_{n-1}/c$ is the classical communication time between qubits $C_{1,2}$ and qubit B where S_{n-1} is the distance between $C_{1,2}$ and B on repeater level n .

has to wait until an operation on another qubit is finished or until a classical signal arrives it undergoes dephasing \mathcal{E}_0 . Fig. 4 shows entanglement swapping between two entangled pairs $A - C_1$ and $C_2 - B$ of qubits. The goal is to teleport the state of qubit C_1 to qubit B by using the entanglement of the pair $C_2 - B$. In a noiseless version of this circuit qubit A would be simply represented by a straight line, which is disconnected from the remaining qubits, and undergoes no operations (and thus it would normally be omitted in the circuit). However, in the presence of noise, it has to wait until the whole procedure is finished and undergoes dephasing during this time. On repeater level n we have to wait a time $t_w = S_{n-1}/c$, where c is the speed of light, until the classical signal resulting from the measurement of qubits C_1 and C_2 arrives at qubit B . For large distances between qubits C_1 , C_2 and B , i.e. on higher repeater levels, this waiting times will be quite long. For instance, taking $S_{n-1} = 1000\text{km}$ yields a waiting time $t_w \approx 3\text{ms}$, which is considerably larger than gate operation times of atomic qubits that are typically in the μs regime, see for instance [31, 32]. Realisations solely based on solid state systems such as electron spins in quantum dots would have even shorter gate operation times [33]. However, in the case of a quantum repeater this is of no advantage since in solid state systems coherence times are typically shorter than in atomic systems where it can exceed 100ms [34, 28]. Since the waiting times during classical communication necessary for entanglement swapping are independent of the implementation, solid state realisations would be less suitable.

If more than two qubit pairs are to be connected we can use a simultaneous entanglement swapping scheme. For example three entangled qubit pairs $A - C_1$, $C_2 - C_3$ and $C_4 - B$, can be transformed into one entangled qubit pair $A - B$ by teleporting the state of qubit C_2 to qubit A (using the entanglement of $A - C_1$) and by teleporting the state of qubit C_3 to qubit B (using the entanglement of $C_4 - B$) at the same time. In general, a sequence of qubit pairs $A - C_1$, $C_2 - C_3$, \dots , $C_{2L_n} - B$ with L_n even can be transformed into a single entangled qubit pair $A - B$ by simultaneously teleporting the state of qubit C_{L_n} to C_{L_n-2} and the state of qubit C_{L_n+1} to C_{L_n+3} before C_{L_n-2} is teleported to C_{L_n-4} and C_{L_n+3} to C_{L_n+5} and so on. If L_n is odd we start by teleporting C_{L_n-1} to C_{L_n-3} and C_{L_n} to C_{L_n+2} before C_{L_n-3} is teleported to C_{L_n-5} and C_{L_n+2} to C_{L_n+4} and so on. This leads to two remaining entangled qubit pairs $A - C_{2L_n-1}$ and $C_{2L_n} - B$ which can be connected to a single pair $A - B$ via the

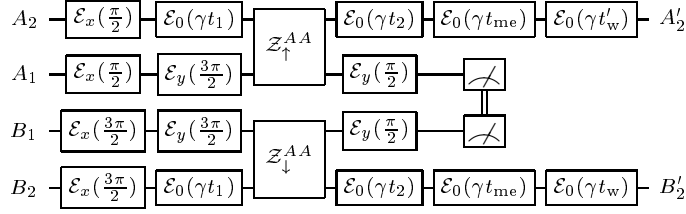


Fig. 5. Quantum circuit for an entanglement purification step. The waiting times are given by $t_1 = 3t_2 = 3\pi/4\Omega$, $t_w = S_n/c$, where S_n is the distance between the qubits $A_{1,2}$ and $B_{1,2}$ on repeater level n , t_{me} is the time required to perform a measurement and $t'_w = t_w + \pi/2\Omega$.

procedure shown in Fig. 4. In total this method takes a time $\lceil L_n/2 \rceil (t_{sw} + S_{n-1}/c)$ where t_{sw} is the time of the operation shown in Fig. 4 minus the classical communication time t_w and $\lceil \cdot \rceil$ is the ceiling function.

Fig. 5 shows the quantum circuit for an entanglement purification step of a qubit pair. The circuit corresponds to the scheme proposed by Deutsch *et al.* [8], but here it is expressed in terms of operations which correspond to our gate and error model. We start with two entangled pairs $A_1 - B_1$ and $A_2 - B_2$ and sacrifice the pair $A_1 - B_1$ in order to get—whenever we obtain a coincidence in the measurements—a new pair $A'_2 - B'_2$, which can have a higher entanglement fidelity than the pair $A_2 - B_2$. Whether the fidelity increases depends on the noise strength and the fidelity of the input pairs and will be discussed in Sec. 4. If we do not get coinciding measurement results the procedure fails and has to be repeated with a new set of pairs. The measurement result has to be classically exchanged between node A (the location of qubits $A_{1,2}$) and node B (the location of qubits $B_{1,2}$), which are a macroscopic distance apart from each other. This is indicated by the double wire connecting the two measurements in Fig. 5. The classical communication time is given by $t_w = S_n/c$ and will thus be, as in the case of entanglement swapping, quite large on higher repeater levels leading to a significant dephasing of qubit A'_2 and B'_2 .

In addition to the already discussed waiting times during entanglement swapping and purification there will be further waiting times for entangled qubits during the repeater protocol: After an entangled pair on repeater level n is created we have to wait a certain time until a second pair is available that we can use for a purification step. In the following, we derive a lower bound for these waiting times.

On the lowest repeater level photons are sent to the repeater nodes and their state is transferred to atomic qubits. The traveling time of the photons can be omitted since they can be triggered such that they arrive at the nodes just in time before a transfer is possible. After the transfer, which consumes a time t_0 , entanglement swapping is performed L_1 times taking a total time $t'_0 = t_0 + \lceil L_1/2 \rceil (t_{sw} + S_0/c)$, where we take $t_{sw} = 9\pi/4\Omega + \pi/4\Omega_{zz} + t_{me}$. The resulting state is then transferred to another qubit pair in a time $t_{tr} = 5\pi/2\Omega + \pi/2\Omega_{zz}$. Only after this transfer is complete, it is possible to transfer photonic states to atomic qubits again and connect them. These pairs are then used to purify the pair previously generated, which takes a time $t_{pur} = 5\pi/2\Omega + \pi/4\Omega_{zz} + t_{me}$ for the operations and measurements, and a time S_1/c for the classical communication of the measurement outcome. During this communication, we can already start creating a subsequent pair necessary for purification,

such that the second purification step can be started after a delay $t_{\text{pur}} + \max(t'_0, S_1/c)$. The purification is performed K_1 times and thus the minimum time it takes to create a pair on repeater level 1 is given by

$$t_1 = t_{\text{tr}} + t'_0 + K_1 [t_{\text{pur}} + \max(t'_0, S_1/c)] . \quad (13)$$

During this process, the pairs on level 1 might have to wait until subsequent pairs for purification are created. After each purification step, this additional waiting time is given by $t_{\text{aw}} = \max(0, t'_0 - S_1/c)$.

On higher levels, the minimum additional waiting time can be estimated as follows. In order to create a pair on level $n \geq 2$ one has to create $\prod_{m=2}^n (K_m + 1)$ times the pairs on level 1, which takes at least a time

$$t_n = t_1 \prod_{m=2}^n (K_m + 1). \quad (14)$$

However, while the pairs created on level $n - 1$ are used to purify the pairs on level n , we can already start to prepare the pairs on level $n - 2$, $n - 3$, and so on. Hence, the minimum time the pairs on level n have to wait for the completion of the pairs on level $n - 1$ is given by

$$t_{n-1}^c = \max \left\{ 0, t_{n-1} - \sum_{l=1}^{n-2} t_l \right\} \quad (15)$$

for $n \geq 2$ and $t_0^c = t_0$. The minimum additional waiting time after each purification and transfer step on level n is then given by

$$t_{\text{aw}} = \max \{ 0, \lceil L_n/2 \rceil (t_{\text{sw}} + S_{n-1}/c) + t_{n-1}^c - S_n/c \} \quad (16)$$

and

$$\tilde{t}_{\text{aw}} = \lceil L_n/2 \rceil (t_{\text{sw}} + S_{n-1}/c) + t_{n-1}^c, \quad (17)$$

respectively. Note that in Eq. (16) the waiting time $t_w = S_n/c$ has been subtracted from the additional waiting time t_{aw} , since it is already included in the purification scheme, see Fig. 5.

Equation (14) can be used to estimate the operation time for the quantum repeater. It provides only a lower bound since it gives the time if the operation of the repeater was successful “in one go”, i.e., if all involved purification steps have been successful. However, the probability for this to happen is extremely small [11] and most likely one would operate the repeater in a different way, such that on each repeater level one would wait until the corresponding purification steps are successful, which introduces further waiting times.

3.2 Error model for DFS qubits

The setup we consider for an experimental implementation of the repeater nodes utilises single atoms stored in neighbouring dipole traps, such as the wells of an optical lattice [13]. Recent experiments [18, 19, 20, 21, 28] showed that for this case the coupling of the qubits to their environment, for example caused by electric or magnetic stray fields, can be considered to be homogeneous, that means identical for all qubits. Thus it is possible to extend the lifetime of the stored information considerably by encoding it in a DFS, which protects the qubits from homogeneous noise. In the next subsection, we briefly discuss two possible DFSs which we

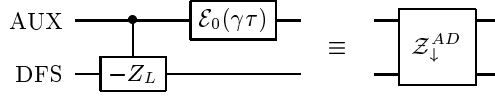


Fig. 6. Noisy controlled- $(-Z)$ operation, Z_{\downarrow}^{AD} , between an auxiliary qubit and a DFS qubit. In reality the dephasing takes place during the gate operation. In simulations it can be applied before or after the controlled- $(-Z)$ operation.

consider in this paper. The first DFS scheme, which was used in Ref. [13], encodes a logical qubit in four two-level atoms in such a way that it is protected against arbitrary kinds of homogeneous noise [17]. The second DFS scheme employs only two atoms, and is therefore easier to realise, but protects the encoded quantum information only against homogeneous dephasing. However, this is sufficient for a lot of implementations, as has already been demonstrated in experiments [18, 19, 20, 21]. For both cases we present how the single and two qubit gates necessary for implementing the repeater protocol can be performed and which limitations occur.

3.2.1 Single qubit gates, two qubit gates and measurements of DFS qubits

The two logical states of a DFS qubit are represented by two states of a system consisting of four two-level atoms, which are stored in an array of dipole traps,

$$\begin{aligned} |0\rangle_{\text{DFS}} &= \frac{1}{2}(|01\rangle - |10\rangle) \otimes (|01\rangle - |10\rangle), \\ |1\rangle_{\text{DFS}} &= \frac{1}{2\sqrt{3}}(2|1100\rangle + 2|0011\rangle - (|01\rangle + |10\rangle)^{\otimes 2}), \end{aligned} \quad (18)$$

where $|ijkl\rangle = |i\rangle_1|j\rangle_2|k\rangle_3|l\rangle_4$ with $i, j, k, l = 0, 1$ are the basis states of the four-atom system. This subspace does not couple to collective noise corresponding to fluctuating fields of the form

$$H_I = \sum_{i=1}^4 \sigma_i^x B_x + \sigma_i^y B_y + \sigma_i^z B_z. \quad (19)$$

As a consequence, the subspace is immune to all kinds of homogeneous noise. So far the DFS in equation (18) has not been implemented using an atomic system. There are, however, experimental realisations of a DFS which protects qubits against homogeneous dephasing [18, 19, 20, 21] using the simpler DFS described below. It has been demonstrated that the coherence time of quantum information stored in such a DFS is ultimately limited by the lifetime of the excited atomic level with respect to spontaneous decay [19, 20]. The lifetime of ground state hyperfine levels with respect to spontaneous decay is extremely long, in fact times exceeding 10 minutes have been observed [21]. We can therefore neglect uncorrelated spontaneous emission and assume that quantum information is stored without loss in the DFS.

It was shown in [13] that single qubit rotations $R_x(\theta)$ and $R_z(\theta)$ can be done without leaving the decoherence free subspace and thus we assume that these operations are performed without any error. In contrast to this it was shown that a feasible implementation of a two qubit gate can be achieved by applying a controlled- $(-Z)$ operation, which involves the use of an unprotected auxiliary atom. The five atoms are then subject to collective noise of

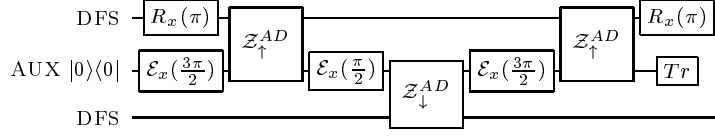


Fig. 7. Implementation of a controlled- $(-Z)$ operation, $\mathcal{Z}_{\downarrow}^{DD}$, between two DFS qubits.

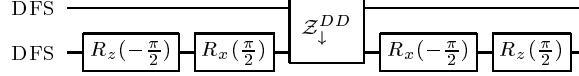


Fig. 8. Quantum circuit for a controlled-not operation, $\mathcal{X}_{\downarrow}^{DD}$, between two logical qubits.

the form $H_I + \sigma_{\text{AUX}}^x B_x + \sigma_{\text{AUX}}^y B_y + \sigma_{\text{AUX}}^z B_z$ and the action of this operator on a state $|\psi\rangle_{\text{DFS}}|\phi\rangle_{\text{AUX}}$ is given by $|\psi\rangle_{\text{DFS}}|\phi\rangle_{\text{AUX}} \rightarrow |\psi\rangle_{\text{DFS}}(\sigma_{\text{AUX}}^x B_x + \sigma_{\text{AUX}}^y B_y + \sigma_{\text{AUX}}^z B_z)|\phi\rangle_{\text{AUX}}$. Hence, we can assume that the noise acts independently on the auxiliary atom. We further restrict our considerations to dephasing noise $B_z \sigma_{\text{AUX}}^z$. The dynamics of the auxiliary atom is thus described by the model detailed in Sec. 3. Since the noise operation (dephasing of the auxiliary atom) and the controlled- $(-Z)$ operation commute, the combined operation can be represented by an effective operation as shown in Fig. 6, where τ is the time needed to perform the controlled- $(-Z)$ gate. In the following figures we denote this gate as $\mathcal{Z}_{\downarrow}^{AD}$, the arrow again defining control and target qubit. Since τ is relatively large (~ 1 ms) we expect decoherence caused by the auxiliary atom to be the major limiting factor in our setup, because the long waiting times of the qubits during classical communication between the repeater nodes do not play any role for the DFS qubits.

Although Ref. [13] concentrates on a DFS given by Eq. (18), we point out that in the case where only collective dephasing (i.e. $B_x = B_y = 0$) is the relevant source of noise a DFS consisting of two atoms is sufficient. In this case, the logical states are

$$\begin{aligned} |0\rangle_{\text{DFS}} &= \frac{1}{\sqrt{2}}(|01\rangle + |10\rangle), \\ |1\rangle_{\text{DFS}} &= \frac{1}{\sqrt{2}}(|01\rangle - |10\rangle). \end{aligned} \quad (20)$$

The controlled- $(-Z)$ operation between an auxiliary (atomic) qubit and a DFS qubit as well as rotations $R_z(\theta)$ can be done in exactly the same way as described in Ref. [13] (omitting two of the four atoms) with the same fidelities and operation times. Rotations $R_x(\theta)$ can be performed using a laser to induce a rotation around the z -axis of the Bloch sphere of, e.g., the first atom constituting the DFS. As in the case of the four-qubit DFS, these operations can be done without leaving the DFS and noise is mainly introduced by the auxiliary atom. Hence, all methods and results presented in this paper are also valid for the DFS spanned by the states given in Eq. (20).

The operation depicted in Fig. 6 can be used to implement controlled operations between two DFS qubits by using an auxiliary qubit. Fig. 7 shows a possibility to implement a controlled- $(-Z)$ gate between two DFS qubits. The single qubit operations and the measurement of the auxiliary qubit are the same as in Sec. 3.1. The controlled- $(-Z)$ operation

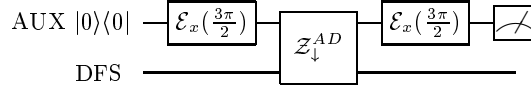


Fig. 9. Measurement of a DFS qubit.

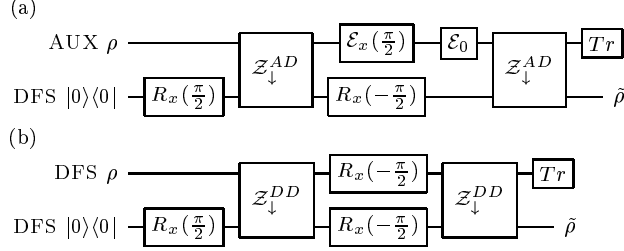


Fig. 10. Quantum circuits for the transfer of (a) the state of an atomic qubit to a DFS qubit and (b) the state of a DFS qubit to a DFS qubit. The operation \mathcal{E}_0 shown in (a) has no effect on the outcome of the state transfer, see text. In the noiseless case the output state $\tilde{\rho}$ would be equal to the input state ρ .

can then be used to generate a controlled-not between two DFS qubits as shown in Fig. 8. Analogously to our previous notation, these are denoted in the following figures as $\mathcal{Z}_{\downarrow}^{DD}$ and $\mathcal{X}_{\downarrow}^{DD}$.

In order to measure the state of a DFS qubit we again make use of an auxiliary qubit. The corresponding circuit is shown in Fig. 9. The measurement of the auxiliary qubit is equivalent to a measurement of the DFS qubit.

3.2.2 Building blocks of the quantum repeater using DFS qubits

The basic modules necessary to implement a quantum repeater involving DFS qubits are shown in Figs. 10-12. In the case of state transfer shown in Fig. 10 we need two procedures, namely a transfer from an auxiliary qubit to a DFS qubit and a transfer of the state from one DFS qubit to another one. In contrast to the state transfer between two DFS qubits (and also between two unprotected qubits, see Fig. 3), which can theoretically be avoided, the transfer between auxiliary (atomic) qubit and DFS qubit is necessary on the lowest level of the quantum repeater. This is required since we assume that the state of the flying qubit (typically a photon) is first transferred to an atom, see Sec. 2 and Ref. [13], and not directly to a DFS qubit. The circuit shown in Fig. 10a includes a dephasing operation, which accounts for the fact that the first qubit has to wait until the $R_x(-\pi/2)$ gate on the second qubit is finished. This operation is relatively slow (~ 2.5 ms) [13] and is thus much slower than typical single qubit gates on atomic (auxiliary) qubits. However, since the \mathcal{E}_0 operation commutes with the $\mathcal{Z}_{\downarrow}^{AD}$ operation, this noise has no effect on the outcome of the state transfer.

The quantum circuit for entanglement swapping with DFS qubits is shown in Fig. 11. The principle is the same as described in Sec. 3.1.3: The state of qubit C_1 is teleported to qubit B using the entanglement of the pair $C_2 - B$. Since quantum information can be stored in the DFS without losses, waiting times during classical communications do not have any effect if they do not exceed the coherence time of the DFS qubit (see above). Thus qubit A is omitted in this circuit since it would be simply represented by a straight line.

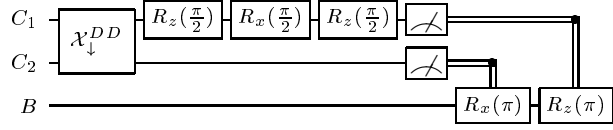


Fig. 11. Quantum circuit for entanglement swapping involving only DFS qubits. The shown circuit corresponds to the standard protocol of teleporting the state of qubit C_1 to qubit B .

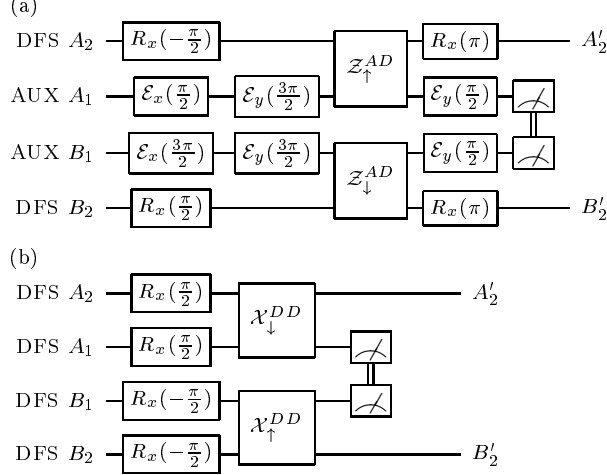


Fig. 12. Quantum circuit for an entanglement purification step between (a) pairs of auxiliary and DFS qubits and (b) two pairs of DFS qubits.

Figure 12 shows the quantum circuit for entanglement purification of (a) a pair of auxiliary qubits $A_1 - B_1$ and a pair of DFS qubits $A_2 - B_2$, and (b) two pairs of DFS qubits $A_1 - B_1$ and $A_2 - B_2$. The major difference to the corresponding case of unprotected qubits (Fig. 5) is again that the waiting times during classical communication do not have any effect if they are shorter than the coherence time of the DFS qubit.

4 Results of simulations

In this section, we present results of simulations of the full nested purification protocol. For a better understanding we first concentrate on its main components, namely entanglement swapping and entanglement purification, as well as state transfer. As indicated in Sec. 2 the state transfer is theoretically not necessary, however it turns out that its inclusion into the repeater protocol does not reduce the final entanglement fidelity significantly. Therefore, we include the state transfer into the repeater protocol since in an experimental implementation it might be easier to do so.

We assume that the initial states are either Werner states

$$\rho_W = f_0 |\Phi_+\rangle\langle\Phi_+| + \frac{1-f_0}{3} (|\Phi_-\rangle\langle\Phi_-| + |\Psi_+\rangle\langle\Psi_+| + |\Psi_-\rangle\langle\Psi_-|) \quad (21)$$

or binary (mixture) states

$$\rho_B = f_0 |\Phi_+\rangle\langle\Phi_+| + (1-f_0) |\Phi_-\rangle\langle\Phi_-|, \quad (22)$$

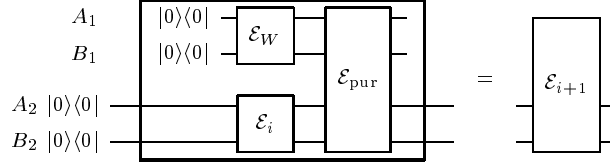


Fig. 13. Illustration of the numerical method taking entanglement purification with Werner states as an example. The operation in the big box can be combined via process tomography to a single operation \mathcal{E}_{i+1} given by a set of Kraus operators. Initially we have $\mathcal{E}_0 = \mathcal{E}_W$. The method is repeated n times corresponding to n entanglement pumping processes. For more details see text.

where

$$|\Phi_{\pm}\rangle = \frac{1}{\sqrt{2}}(|00\rangle \pm |11\rangle), \quad |\Psi_{\pm}\rangle = \frac{1}{\sqrt{2}}(|01\rangle \pm |10\rangle). \quad (23)$$

The entanglement fidelity of a state ρ is defined as

$$f = \langle \Phi_+ | \rho | \Phi_+ \rangle. \quad (24)$$

In order to simulate the repeater and its constituents we developed a program with a modular structure, i.e., it allows the simulation of a quantum circuit by successively applying subroutines with mixed states as input. Each of these subroutines corresponds to a quantum operation (gates and measurements), which is represented by a Kraus decomposition. Furthermore, we extensively use the fact that a quantum network can be combined into one effective quantum operation, the Kraus operators of which can be calculated by using the quantum process tomography algorithm [35].

We illustrate this method in more detail for the example of entanglement purification with Werner states as shown in Fig. 13. The aim is to purify a qubit pair $A_2 - B_2$ via entanglement pumping using Werner states. The operation \mathcal{E}_W creates a Werner state out of the input state $|00\rangle\langle 00|$ and the operation \mathcal{E}_{pur} corresponds to the actual entanglement purification circuit, for example as shown in Fig. 5. The operation \mathcal{E}_i is set initially to $\mathcal{E}_0 = \mathcal{E}_W$. The circuit shown in Fig. 13 then leads to an output state which corresponds to the state after one entanglement pumping process. All the operations inside the large box in Fig. 13 can be combined to one effective quantum operation \mathcal{E}_1 , which acts on two qubits and which can be determined via process tomography. The operation \mathcal{E}_1 is then used instead of \mathcal{E}_0 in a repetition of these steps and so forth. After n iterations we get an effective operation \mathcal{E}_n which, when applied to the input state $|00\rangle\langle 00|$, creates a state that we would get after n entanglement pumping steps. By replacing the quantum operations inside the large box in Fig. 13 appropriately, we applied this method also to state transfer and entanglement swapping, since in all cases all but two qubits are measured at the end of the operation, i.e., also transfer and swapping can be represented by an effective operation with two input and two output qubits. Ultimately, the combination of state transfer, entanglement swapping, and purification makes it possible to calculate an effective quantum operation for the whole repeater, which transforms a given input state (e.g. $|00\rangle\langle 00|$) into the final state of the repeater.

For the examples shown in this section we set $\Omega = \Omega_x = \Omega_y = \Omega_z = 2\pi \times 50\text{kHz}$, which means we assume that a 2π -rotation around the x, y, z axes can be done in $10\mu\text{s}$. The two particle interaction strength of Eq. (11) is set to $\Omega_{zz} = 0.1\Omega$, i.e., the controlled- Z gate

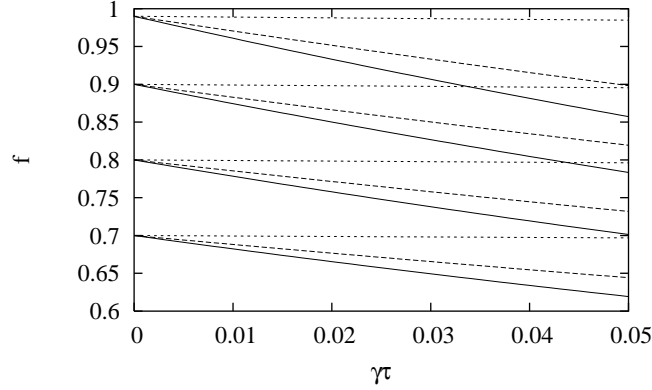


Fig. 14. Fidelities after transfer of the state of a qubit pair depending on the noise parameter γ ($\tau = 1\text{ms}$). The initial states are Werner states with fidelities $f_0 = 0.7, 0.8, 0.9, 0.99$ (bottom to top). Dotted lines correspond to the transfer of auxiliary (unprotected) qubits (cf. Fig. 3), dashed lines correspond to a transfer from auxiliary to DFS qubits (cf. Fig. 10a) and solid lines correspond to the transfer of DFS qubits (cf. Fig. 10b).

described in Fig. 2 takes $32.5\mu\text{s}$. Furthermore, we assume an operation time for the controlled- $(-Z)$ operation between an auxiliary qubit and a DFS qubit (see Fig. 6) of $\tau = 1\text{ms}$, which corresponds to the gate operation times calculated in Ref. [13]. The measurement time is set to $t_{\text{me}} = 10\mu\text{s}$ and the measurement error is assumed to be $1 - \eta = 0.01$ unless otherwise stated.

Figure 14 shows the fidelity of the state of an entangled particle pair after it was transferred to another qubit pair versus γ by means of the circuits described in the previous section. The initial states are Werner states. The corresponding plot for binary states (not shown) is very similar and deviates from Fig. 14 appreciably only for small fidelities. Assuming a coherence time of $1/\gamma = 100\text{ms}$, the initial fidelity is reduced by $\sim 0.1\%$ in the case of a transfer between auxiliary qubits, by $\sim 1 - 2\%$ for a transfer from auxiliary to DFS qubits and by $\sim 2 - 3\%$ in the case of a transfer between DFS qubits.

The fidelities after connecting $L + 1$ entangled qubit pairs (i.e., after L connection processes) via entanglement swapping are shown in Fig. 15. In these examples we assumed that there are initially $L + 1$ qubit pairs of fidelity f_0 and distance l_0 in a Werner state (Fig. 15a) or in a binary state (Fig. 15b), which are connected according to the method described in Sec. 3.1.3. This implies that the i th entangled pair with $i = 1, 2, \dots, L + 1$ has to wait an additional time $\max\{0, \lceil (L + 1)/2 \rceil - i\} (l_0/c + t_{\text{sw}})$, until the connection process starts for this pair. The final pair has then a distance of $(L + 1)l_0$.

As can be seen from these plots, entanglement swapping with partially entangled states leads to a significant loss of fidelity, in fact it has been shown that the fidelity decreases exponentially in the noiseless case [11]. The effect of noisy gate operations and waiting times becomes less important for small fidelities. For example, starting with two Werner pairs of fidelity 80% we lose about 15% fidelity by connecting them. For short distances a swapping procedure using unprotected qubits performs generally better than one with DFS qubits due to the long gate operation times in the decoherence-free case. However, for distances l_0 larger than about 1000km entanglement swapping with DFS qubits becomes advantageous.

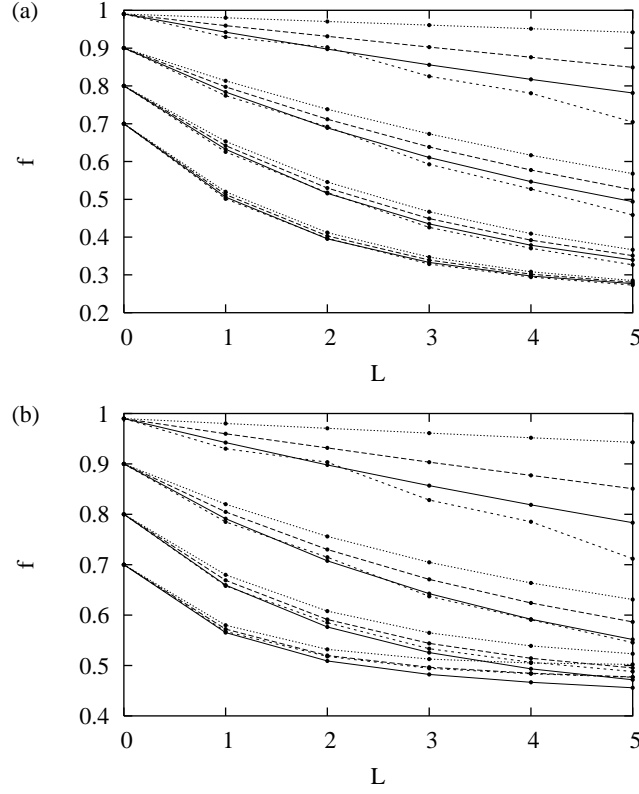


Fig. 15. Fidelities depending on the number of connection processes L for $\gamma = 1/100$ ms. The qubit pairs are initially (a) in Werner states and (b) in binary states with fidelities $f_0 = 0.7, 0.8, 0.9, 0.99$ (bottom to top). The solid lines correspond to DFS qubits, and the short dashed and long dashed lines correspond to auxiliary (unprotected) qubit pairs with distances of $l_0 = 1000$ km and $l_0 = 10$ km, respectively. The dotted line corresponds to the noiseless case, i.e., $\gamma = 0, \eta = 1$.

The effect of entanglement purification (using entanglement pumping) of an entangled qubit pair, which has initially the fidelity f_0 , is shown in Fig. 16 and Fig. 17. In particular, we calculated the maximally reachable fidelity f_{\max} after a large number of successful purification steps depending on f_0 , which is also the fidelity of the successively provided additional pairs used for entanglement pumping. In Figs. 16 and 17 the initial pair and the additional pairs are Werner states and binary states, respectively. Whenever the curves are above the bold diagonal line we gain fidelity, otherwise the fidelity is decreased during the process. These figures illustrate again that the DFS scheme becomes better than the scheme based on unprotected qubits at a distance of $l_0 \approx 500$ km. For $\gamma = 1/25$ ms and a distance of $l_0 = 1000$ km (lowest short dashed line in Fig. 16b) purification would not be possible at all for unprotected qubits. Moreover, binary states perform generally better than Werner states [9]. Also shown in these figures are the maximal fidelities for purification between an auxiliary qubit and a DFS qubit (long dashed lines), which is needed on the first level of the DFS repeater, compare Fig. 12a. Note that in this case the maximally reachable fidelity, i.e., the point where the curves intersect the diagonal line in the upper right corner of the plots,

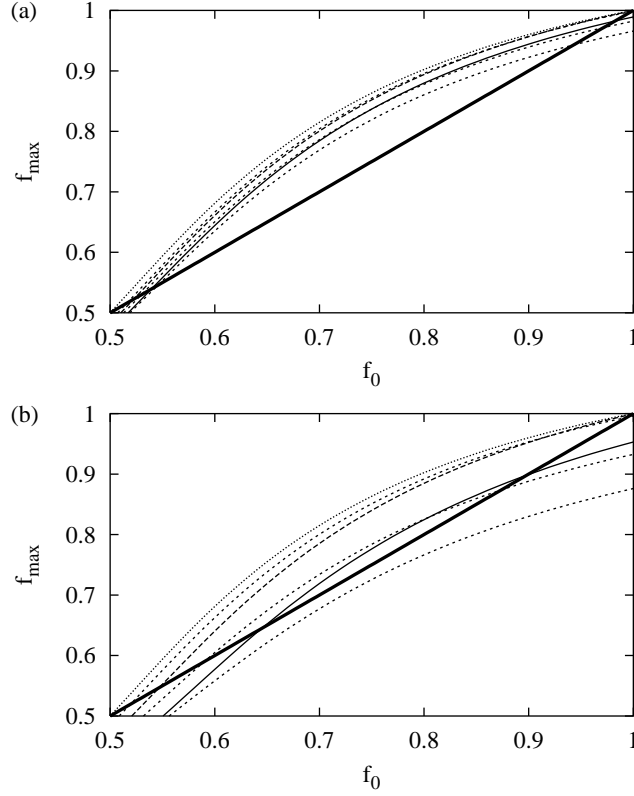


Fig. 16. Maximal fidelity obtainable via entanglement purification using Werner states versus initial fidelity f_0 , which is also the fidelity of the successively generated entangled pairs, for (a) $\gamma = 1/100\text{ms}$ and (b) $\gamma = 1/25\text{ms}$. The bold, diagonal lines aid to read off whether entanglement is gained or lost, see text. The thin, solid lines correspond to purification using DFS qubits, and the short dashed lines correspond to purification using unprotected qubits for $l_0 = 10\text{km}$, 500km , 1000km (top to bottom). The long dashed line was obtained by purifying a DFS qubit pair with an auxiliary (unprotected) qubit pair. As a reference we also plotted the corresponding result for the noiseless case (dotted lines).

is very close to one even for small coherence times $1/\gamma$. The points where the curves intersect the bold diagonal line in the lower left corner correspond to the purification threshold below which no purification is possible.

As described in Sec. 2, the quantum repeater protocol we use in this paper is a nested arrangement of entanglement purification and entanglement swapping. The DFS repeater suffers from long gate operation times, which particularly affects the noisy two qubit gate. Quantum gates based on unprotected qubits are significantly faster, however, due to long waiting times during the repeater protocol in the case of long distances, the involved memory qubits are strongly prone to decoherence. In Fig. 18 we show an example which compares these two cases. We calculated the fidelity of the entangled pair generated by a quantum repeater with n levels. On each level we perform 5 purification steps and perform one connection (i.e., $L_j = 1$) except for the first level where no connection is done (i.e., $L_1 = 0$). For the repeater based on unprotected qubits we assume $t_0 = 10\mu\text{s}$. The distance of the generated

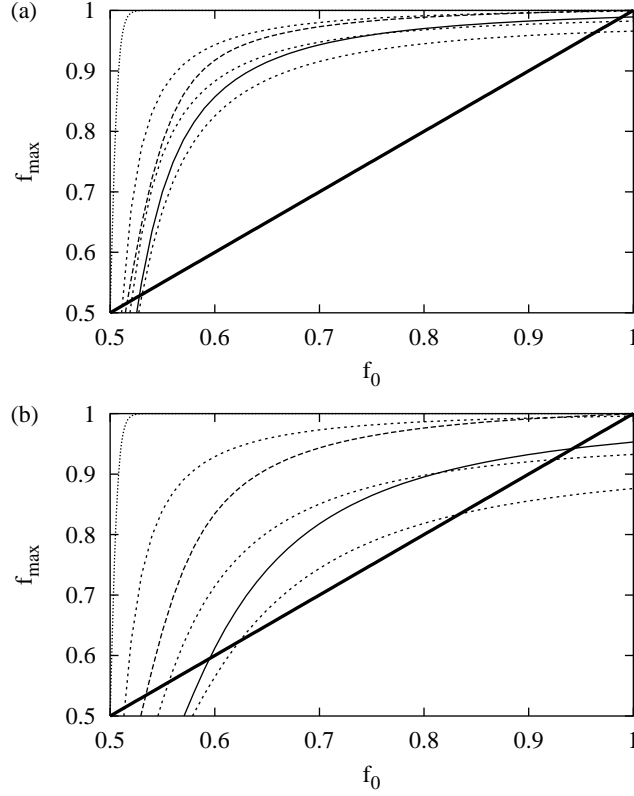


Fig. 17. Same as in Fig. 16 but using binary states instead of Werner states.

entangled pair on level n scales like $S_n = 2^{n-1}l_0$. If we take for example $l_0 = 10\text{km}$ and $n = 12$, we get a distance of 20480km. Clearly, we do not suggest that the distance over which entangled pairs can be distributed with the DFS quantum repeater is unlimited. The DFS we use protects only against noise given by Eq. (19) and is for example not immune to fluctuating inhomogeneous fields. Therefore, the “decoherence free” subspace ultimately has a finite coherence time which, however, can be very long (see Sec. 3.2.1). In particular, we expect it to exceed the time necessary to generate an entangled pair on an intercontinental distance, which is on the order of tens of seconds [9]. As can be seen from Fig. 18, the DFS repeater outperforms the repeater based on unprotected qubits already on repeater level 4 which corresponds to 80km in the above example. The final fidelity of the entangled pairs produced by the DFS repeater is $f = 98.1\%$. The waiting times, which are relevant for the repeater based on unprotected qubits, are calculated according to Eqs. (16) and (17), i.e., they represent a lower bound. We emphasise here that the strategy (i.e., the choice of the L_j , the number of purification steps on a repeater level, the distance l_0 of the initially created pairs etc.) used in this example might not be the most optimal one. A systematic approach to this problem, albeit with a different error model, can be found in [11]. However, it was found in this reference that even with an optimised strategy and reasonable errors intercontinental distances can not be reached by a repeater using entanglement pumping. Therefore, a number

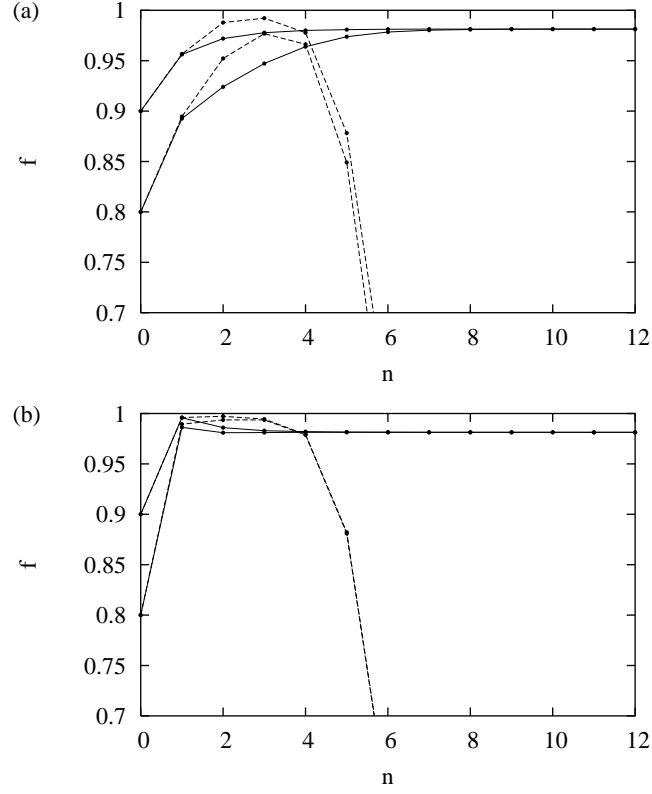


Fig. 18. Fidelity f of an entangled pair created by a quantum repeater using (a) Werner states and (b) binary states on the lowest level depending on the repeater level n . The solid lines correspond to a DFS repeater and the dashed lines to a repeater based on unprotected qubits. The fidelities of the initially created pairs are $f_0 = 0.8, 0.9$ (bottom to top), $l_0 = 10\text{km}$ and $\gamma = 1/100\text{ms}$. For further parameters see text.

of alterations to the repeater protocol have been proposed to increase the distance [11]. Our results show that improving the quantum memory by employing a decoherence free subspace (and not changing the repeater protocol) gives an alternative method to reach intercontinental distances.

5 Conclusions

In the present paper we described in detail the implementation of a quantum repeater based on DFS quantum memories, i.e., the qubits at the repeater nodes are represented by two states of a DFS consisting of four physical qubits, which can be manipulated as proposed in Ref. [13]. We showed that the distribution of entangled pairs over long distances is possible with our setup. We simulated the DFS repeater as well as a repeater based on unprotected qubits using realistic parameters, and demonstrated that the DFS scheme outperforms the scheme based on unprotected qubits if waiting times due to classical communication become too large. The implementation of a repeater based on a reliable memory, even in the case of slow and faulty gate operations as in the example we considered, would thus offer the

possibility for long distance quantum communication.

In future work one might enhance the performance of the quantum repeater even further by conceiving hybrid architectures, which combine the advantages of fast schemes based on unprotected qubits and schemes involving DFS qubits. For example, one could use the DFS qubits merely as a memory and quantum information is processed with unprotected qubits. The memory could be accessed via state transfer mechanisms as it is discussed in the present paper acting as an interface between memory and processing qubits. Fast gate operations would then be performed on and between unprotected qubits. A further option along the lines of these ideas is based on the observation that the maximally reachable fidelity f_{\max} of purification of a DFS qubit pair with unprotected qubit pairs is larger than purification using only DFS qubit pairs (see long dashed lines in Figs. 16 and 17): On the final repeater level(s) we could therefore transfer the state of the DFS qubit pair to an unprotected qubit pair and use this in turn to purify another DFS qubit pair. If the loss in fidelity induced by the state transfer is not too high the results presented in Figs. 16 and 17 suggest that this could lead to final fidelities exceeding those obtained from using exclusively DFS qubits on higher repeater levels.

Acknowledgements

This research was supported by a Marie Curie Intra-European Fellowship within the 6th European Community Framework Programme ('RAQUIN'). This work was also supported by the EPSRC (UK) through the QIP IRC (GR/S82176/01) and project EP/C51933/1 and by the EU through the STREP project OLAQUI. A.K. acknowledges financial support from the Keble Association.

1. N. Gisin, G. Ribordy, W. Tittel, and H. Zbinden (2002), *Quantum cryptography*, Rev. Mod. Phys., 74, p. 145.
2. A. V. Sergienko, ed. (2006), *Quantum Communications and Cryptography*, Taylor and Francis (New York).
3. H.-J. Briegel, W. Dür, J. I. Cirac, and P. Zoller (1998), *Quantum repeaters: The role of imperfect local operations in quantum communication*, Phys. Rev. Lett., 81, p. 5932.
4. L.-M. Duan, M. D. Lukin, J. I. Cirac, and P. Zoller (2001), *Long-distance quantum communication with atomic ensembles and linear optics*, Nature, 414, p. 413.
5. C. H. Bennett, G. Brassard, C. Crépeau, R. Jozsa, A. Peres, and W. K. Wootters (1993), *Teleporting an unknown quantum state via dual classical and Einstein-Podolsky-Rosen channels*, Phys. Rev. Lett., 70, p. 1895.
6. M. Zukowski, A. Zeilinger, M. A. Horne, and A. K. Ekert (1993), *"Event-ready-detectors" Bell experiment via entanglement swapping*, Phys. Rev. Lett., 71, p. 4287.
7. C. H. Bennett, G. Brassard, S. Popescu, B. Schumacher, J. A. Smolin, and W. K. Wootters (1996), *Purification of noisy entanglement and faithful teleportation via noisy channels*, Phys. Rev. Lett., 76, p. 722.
8. D. Deutsch, A. Ekert, R. Jozsa, C. Macchiavello, S. Popescu, and A. Sanpera (1996), *Quantum privacy amplification and the security of quantum cryptography over noisy channels*, Phys. Rev. Lett., 77, p. 2818.
9. W. Dür, H.-J. Briegel, J. I. Cirac, and P. Zoller (1999), *Quantum repeaters based on entanglement purification*, Phys. Rev. A, 59, p. 169.
10. C. H. Bennett, D. P. DiVincenzo, J. A. Smolin, and W. K. Wootters (1996), *Mixed-state entanglement and quantum error correction*, Phys. Rev. A, 54, p. 3824.
11. L. Hartmann, B. Kraus, H.-J. Briegel, and W. Dür (2007), *Role of memory errors in quantum repeaters*, Phys. Rev. A, 75, p. 032310.

12. O. A. Collins, S. D. Jenkins, A. Kuzmich, and T. A. B. Kennedy (2007), *Multiplexed memory-insensitive quantum repeaters*, Phys. Rev. Lett., 98, p. 060502.
13. A. Klein, U. Dörner, C. Moura Alves, and D. Jaksch (2006), *Robust implementations of quantum repeaters*, Phys. Rev. A, 73, p. 012332.
14. P. Zanardi and M. Rasetti (1997), *Noiseless quantum codes*, Phys. Rev. Lett., 79, p. 3306.
15. L.-M. Duan and G.-C. Guo (1998), *Reducing decoherence in quantum-computer memory with all quantum bits coupling to the same environment*, Phys. Rev. A, 57, p. 737.
16. D. A. Lidar, I. L. Chuang, and K. B. Whaley (1998), *Decoherence-free subspaces for quantum computation*, Phys. Rev. Lett., 81, p. 2594.
17. D. Bacon, J. Kempe, D. A. Lidar, and K. B. Whaley (2000), *Universal fault-tolerant quantum computation on decoherence-free subspaces*, Phys. Rev. Lett., 85, p. 1758.
18. D. Kielpinski, V. Meyer, M. A. Rowe, C. A. Sackett, W. M. Itano, C. Monroe, and D. J. Wineland (2001), *A decoherence-free quantum memory using trapped ions*, Science, 291, p. 1013.
19. C. F. Roos, G. P. T. Lancaster, M. Riebe, H. Häffner, W. Hänsel, S. Gulde, C. Becher, J. Eschner, F. Schmidt-Kaler, and R. Blatt (2004), *Bell states of atoms with ultralong lifetimes and their tomographic state analysis*, Phys. Rev. Lett., 92, p. 220402.
20. C. F. Roos, M. Chwalla, K. Kim, M. Riebe, and R. Blatt (2006), *Designer atoms for quantum metrology*, Nature, 443, p. 316.
21. C. Langer, R. Ozeri, J. D. Jost, J. Chiaverini, B. DeMarco, A. Ben-Kish, R. B. Blakestad, J. Britton, D. B. Hume, W. M. Itano, D. Leibfried, R. Reichle, T. Rosenband, T. Schaetz, P. O. Schmidt, and D. J. Wineland (2005), *Long-lived qubit memory using atomic ions*, Phys. Rev. Lett., 95, p. 060502.
22. E. M. Fortunato, L. Viola, J. Hodges, G. Teklemariam, and D. G. Cory (2002), *Implementation of universal control on a decoherence-free qubit*, New J. Phys., 4, p. 5.
23. J. E. Ollerenshaw, D. A. Lidar, and L. E. Kay (2003), *Magnetic resonance realization of decoherence-free quantum computation*, Phys. Rev. Lett., 91, p. 217904.
24. L. Viola, E. M. Fortunato, M. A. Pravia, E. Knill, R. Laflamme, and D. G. Cory (2001), *Experimental realization of noiseless subsystems for quantum information processing*, Science, 293, p. 2059.
25. P. G. Kwiat, A. J. Berglund, J. B. Altepeter, and A. G. White (2000), *Experimental verification of decoherence-free subspaces*, Science, 290, p. 498.
26. M. Mohseni, J. S. Lundeen, K. J. Resch, and A. M. Steinberg (2003), *Experimental application of decoherence-free subspaces in an optical quantum-computing algorithm*, Phys. Rev. Lett., 91, p. 187903.
27. M. Bourennane, M. Eibl, S. Gaertner, C. Kurtsiefer, A. Cabello, and H. Weinfurter (2004), *Decoherence-free quantum information processing with four-photon entangled states*, Phys. Rev. Lett., 92, p. 107901.
28. S. Kuhr, W. Alt, D. Schrader, I. Dotsenko, Y. Miroshnychenko, A. Rauschenbeutel, and D. Meschede (2005), *Analysis of dephasing mechanisms in a standing-wave dipole trap*, Phys. Rev. A, 72, p. 023406.
29. J. I. Cirac and P. Zoller (2004), *New frontiers in quantum information with atoms and ions*, Phys. Today, 57, p. 38.
30. D. Jaksch, H.-J. Briegel, J. I. Cirac, C. W. Gardiner, and P. Zoller (1999), *Entanglement of atoms via cold controlled collisions*, Phys. Rev. Lett., 82, pp. 1975–1978.
31. O. Mandel, M. Greiner, A. Widera, T. Tom, T. W. Hänsch, and I. Bloch (2003), *Controlled collisions for multi-particle entanglement of optically trapped atoms*, Nature, 425, p. 937.
32. M. Riebe, K. Kim, P. Schindler, T. Monz, P. O. Schmidt, T. K. Körber, H. H. W. Hänsel, C. F. Roos, and R. Blatt (2006), *Process tomography of ion trap quantum gates*, Phys. Rev. Lett., 97, p. 220407.
33. G. Burkard (2004), *Theory of solid state quantum information processing*, cond-mat/0409626v2.
34. S. Kuhr, W. Alt, D. Schrader, I. Dotsenko, Y. Miroshnychenko, W. Rosenfeld, M. Khudaverdyan, V. Gomer, A. Rauschenbeutel, and D. Meschede (2003), *Coherence properties and quantum state*

- transportation in an optical conveyor belt*, Phys. Rev. Lett., 91, p. 213002.
35. M. A. Nielsen and I. L. Chuang (2000), *Quantum Computation and Quantum Information*, Cambridge University Press (Cambridge).